Robotica: (2021) volume 39, pp. 1601–1616. © The Author(s), 2021. Published by Cambridge University Press.
doi:10.1017/S0263574720001381

Wrench Capabilities of a Kinematically Redundant Planar Parallel Manipulator

Roger Boudreau†*, Scott Nokleby‡ and Marise Gallant†

†*Université de Moncton*
E-mail: marise.gallant@umoncton.ca
‡*Ontario Tech University*
E-mail: Scott.Nokleby@ontariotechu.ca

(Accepted December 9, 2020. First published online: January 26, 2021)

SUMMARY
This paper presents a methodology to obtain the wrench capabilities of a kinematically redundant planar parallel manipulator using a wrench polytope approach. A methodology proposed by others for non-redundant and actuation-redundant manipulators is adapted to a kinematically redundant manipulator. Four wrench capabilities are examined: a pure force analysis, the maximum force for a prescribed moment, the maximum reachable force, and the maximum moment with a prescribed force. The proposed methodology, which finds the exact explicit solution for three of the four wrench capabilities, does not use optimization and is very efficient.

KEYWORDS: Parallel manipulators; Redundant manipulators; Polytopes; Force/moment capabilities; Wrench performance indices.

1. Introduction

This paper proposes a methodology to obtain the wrench capabilities of a kinematically redundant planar parallel manipulator. The wrench capability of a manipulator is defined as the maximum wrench that can be applied (or sustained) by a manipulator for a given pose based on the limits of the actuators.[1] A wrench capability plot for a given pose represents the applied wrench in all directions.

It is well known that parallel manipulators contain direct kinematic singularities inside its workspace.[2] Both kinematic redundancy and actuation redundancy have been proposed and shown to eliminate singularities within the workspace.

Kinematic redundancy (e.g., see refs. [3–9]) occurs when extra links and actuators are added to the manipulator. Until recently, the addition of actuators to achieve kinematic redundancy led to some actuators mounted in series. A new approach for kinematic redundancy was recently proposed in which a purely parallel kinematic leg is added, thus maintaining the parallelism of the structure.[10,11] The mobility of kinematically redundant manipulators is greater than the number of degrees of freedom and an infinite number of possible solutions to the inverse kinematics problem exists. The wrench capabilities depend on the chosen configuration.

The other main type of redundancy is actuation redundancy (e.g., see refs. [1, 12–14]) and it is achieved either when a normally passive joint in a leg is actuated or when an extra actuated leg is added to the manipulator. An infinite number of possible solutions for the actuator torques is possible to produce a specified output wrench. Figure 1 shows examples of manipulators that are non-redundant, have in-branch actuation redundancy, have additional branch actuation redundancy, and have kinematic redundancy (note in this figure R and P denote revolute joints and prismatic joints, respectively, an underline indicates an actuated joint, and solid circles and empty circles designate

* Corresponding author. E-mail: roger.a.boudreau@umoncton.ca

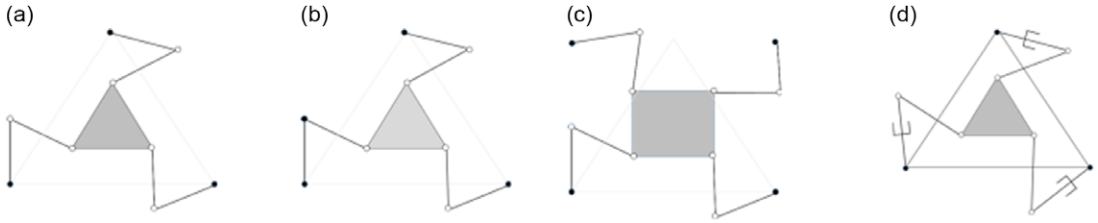

Fig. 1. Manipulator configurations: (a) non-redundant 3-RRR, (b) in-branch actuation redundant 1-RRR–2-RRR, (c) additional-branch actuation redundant 4-RRR, and (d) kinematically redundant 3-RPRR.

actuated and passive joints, respectively). Gosselin and Schreiber[15] present a thorough review of the research pertaining to the different types of redundancy in parallel mechanisms.

The wrench capabilities of a manipulator depend on its design layout, the pose, and the actuator torque capabilities. Three different approaches have been proposed to determine the wrench capabilities: constrained optimization, wrench ellipsoids,[16] and wrench polytopes.[17,18] A thorough presentation of the three approaches is presented by Firmani et al.[18] and is summarized here.

When using a constrained optimization method, an objective function that maximizes the output wrench is optimized such that the static force relation is satisfied subject to the actuator torques remaining within their limits. These methods are normally computationally expensive and may not find the global minimum. It should be noted that the force capability of a non-redundant 3-RRR manipulator (where R denotes a revolute joint) was recently obtained as a closed-form solution using an optimization approach.[19] A Lagrangian function was written that included equality and inequality constraints. The Karush–Kuhn–Tucker conditions were then solved in closed-form to produce the force polytope. When using wrench ellipsoids, the actuator torque vector is bounded by a unit hypersphere in the joint force space. The hypersphere is then linearly mapped into the task wrench space using the static force equation to produce an ellipsoid. As an example, consider a manipulator with two actuators with the same torque capacity, $\tau_{i_{max}} = \pm 1$ Nm . The allowable torques in joint space are represented by a circle and the wrench space is represented by an ellipsoid as shown in Fig. 2(a). However, this circle does not provide the true representation of the torque capacities for the preceding manipulator since the capacities are in reality a square when plotted in joint space, where the corners of the square represent two actuators being at their maximum capacities (either + or – for all combinations) as shown in Fig. 2(b).

Polytopes are generated by mapping a hypercube in joint space (a square for the two-actuator manipulator) into the wrench space using the static force equation, producing a polytope. One can observe that the wrench polytope in the example can be obtained by mapping only the vertices of the torques in joint space into the wrench space. The polytope approach represents the exact mapping of the joint capabilities in the wrench space, while the ellipsoid provides an approximation of the mapping as shown in Fig. 2(c). For a 3-DOF planar manipulator, the torque space is represented as a cube (see Fig. 3). The force polygon for a given pose of the manipulator is simply the intersection of the $f_x - f_y$ plane at M_z with the wrench space as see in Fig. 3.

The force capabilities of redundantly actuated manipulators have been studied by many researchers (e.g., see refs. [1, 20–22]). The force capabilities of kinematically redundant planar parallel manipulators have not received as much attention. The only work found that addressed this problem was that of Weihmann et al..[23] They found the force capability of a 3-RPRR manipulator for a pure force analysis using an optimization approach. They used a Differential Evolution algorithm to obtain the angles of the base revolute joints that maximized the output force applied by the end-effector in a specified direction. The objective function consisted of the satisfaction of the static force relation, the closure of the kinematic chains, and the limits on the actuator torques.The direction of the forces in the force polygon was discretized from 0 to 2π and the objective function had to be optimized for each angle. This method is therefore computationally expensive.

The polytope approach[18] is used in this work to find several wrench capabilities of a kinematically redundant planar parallel manipulator. As stated previously, for a kinematically redundant planar parallel manipulator, the only wrench capability that has been previously published is a pure force analysis (no moment applied). This case is therefore first examined in order to validate and compare with the results of Weihmann et al.[23] and to demonstrate the effectiveness of the proposed method.

https://doi.org/10.1017/S0263574720001381 Published online by Cambridge University Press

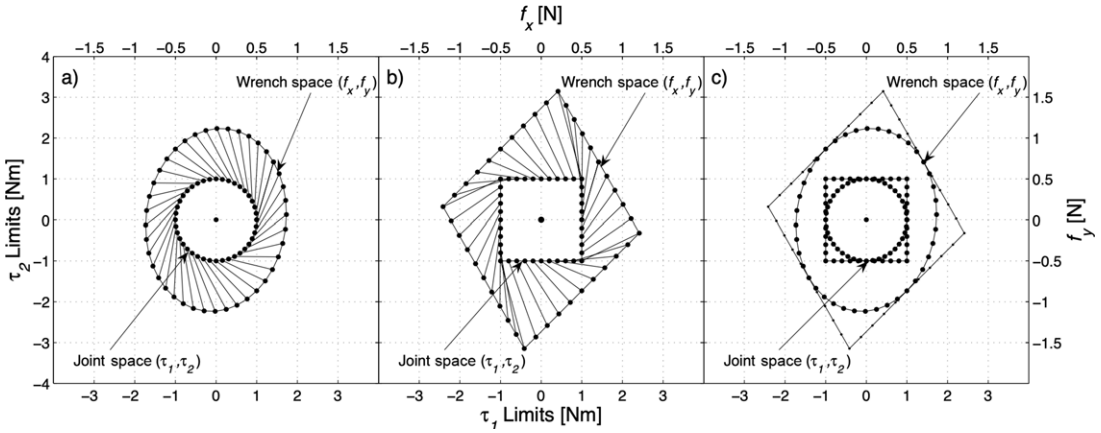

Fig. 2. Mapping of ellipsoids and polytopes from the joint space to the task space.[18]

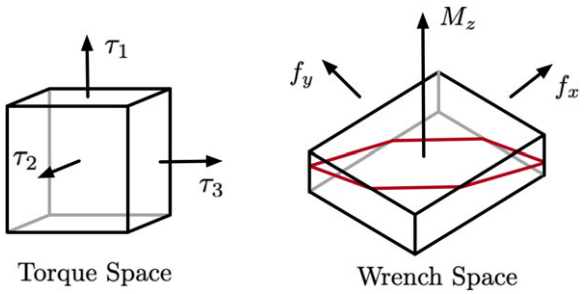

Fig. 3. Mapping of the torque space to the wrench space where the polygon in red is the force polygon for a specified position and moment.

The latter results in an explicit solution to the problem of generating the force polygon and it is therefore computationally efficient. Preliminary results using this method were presented in Boudreau et al..[24] In this work, the method is refined and applied to obtain several other wrench performances for a kinematically redundant planar parallel manipulator.

The outline of the remainder of the paper is as follows: Section 2 discusses force polygons, Section 3 discusses the kinematics of the example manipulator, Section 4 presents the methodology to obtain the wrench performance for kinematically redundant parallel manipulators, Section 5 presents different wrench capabilities for the example manipulator, and Section 6 concludes the paper.

2. Force Polygons

2.1. Force polygon for the 3-RRR manipulator

Figure 4 shows the force polygon of a 3-RRR manipulator when the end-effector is located at the origin of the fixed axes with an orientation of 0°. Many studies can be found in the literature for this manipulator. For example, researchers have optimized its kinematic characteristics,[25] analyzed its singularities,[26] presented a method for its synthesis to obtain a singularity free workspace,[27] and developed simulation tools.[28] A sketch of the manipulator is superimposed on the force polygon for a clearer understanding of what the force polygon represents. For this manipulator, the base edge length is 0.5 m, the moving platform edge length is 0.2 m, the lengths of the first and second links of each leg are 0.2 m, and the actuator torque limits are ±4.2 Nm.[23,29] At the position shown in the figure, the force polygon indicates the maximum force the end-effector can apply (or sustain) in a direction α. The lines in Fig. 4(b) indicate that the actuators are at their maximum torque values. In a given direction (e.g., the dashed line), the force is limited by the actuator torque capabilities. The force in the direction indicated is attained when actuator 3 attains its maximum capacity. The other points on this line (marked with a +) are unattainable since one or more actuators would have to surpass its maximum capacity. The sets of parallel lines correspond to positive and negative torques of the actuators ($\pm\tau_{i_{max}}$). It should be noted that there are 12 intersection points of the lines that

https://doi.org/10.1017/S0263574720001381 Published online by Cambridge University Press

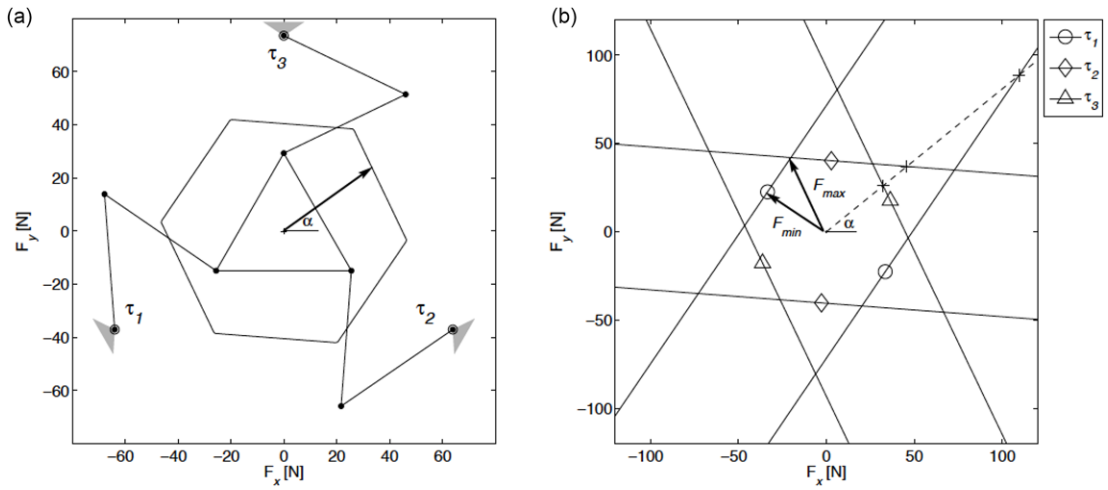

Fig. 4. Force polygon.[29]

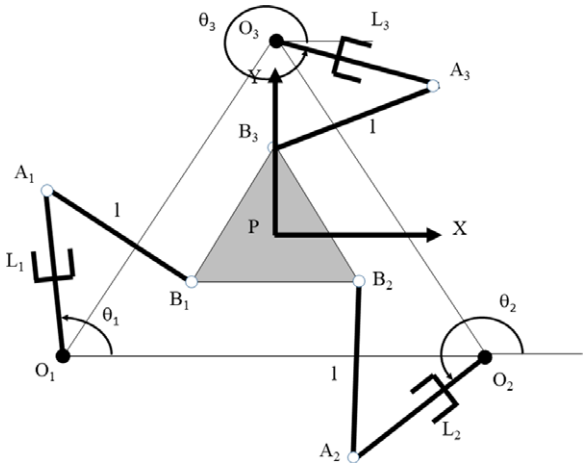

Fig. 5. 3-RPRR manipulator.

correspond to the maximum torques which are the 12 possible combinations of $(\pm\tau_{i_{max}}, \pm\tau_{j_{max}})$, $i \neq j$. Six of the combinations are dismissed since some of the actuators cannot apply the required torque corresponding to these points. At a vertex, two actuators are at their maximum capacities.

The minimum distance between the origin and the lines of the force polygon, represented as F_{min} in Fig. 4(b), represents the force that can be applied in any direction. Some authors call this the isotropic force. The maximum distance between the origin and the lines of the force polygon, represented as F_{max} in Fig. 4(b), represents the largest force that can be applied by the manipulator. The procedure to obtain the force polygon is explained later.

2.2. *Effect of kinematic redundancy on the force polygon*

The kinematically redundant manipulator under study is the 3-RPRR manipulator (see Fig. 5). When the prismatic joints are fixed, it becomes the well-known 3-RRR manipulator. The origin of the fixed frame of reference is located at the geometric center of the triangle formed by the fixed base revolute joints and is denoted by O (not shown). The moving frame is attached to the end-effector at its geometric center, and its origin is denoted by P. In the figure, P and O are coincident in the position shown. The dimensions of the 3-RPRR manipulator are the same as those of the 3-RRR manipulator used by Firmani et al.[29] with the prismatic joints having a nominal length of 0.2 m and are able to adjust ±0.05 m as per.[23] It is assumed that the prismatic joint force limits are large enough to sustain the force produced in the proximal links when the base revolute actuators are at their maximum values.

https://doi.org/10.1017/S0263574720001381 Published online by Cambridge University Press

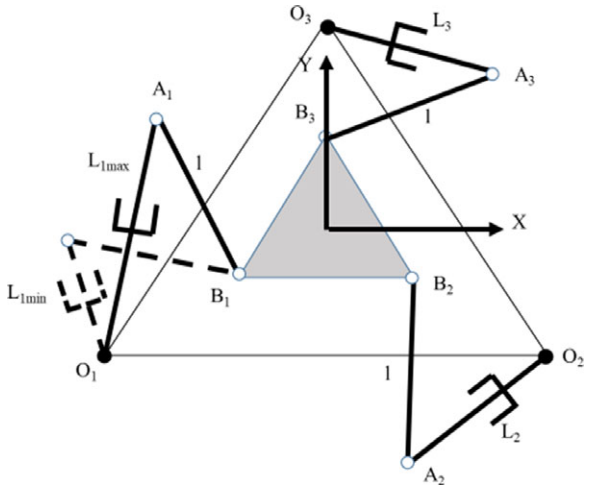

Fig. 6. Effect of kinematic redundancy on the first leg.

Figure 6 shows the effect of kinematic redundancy using the first leg as an example. The figure shows the leg when the prismatic joint is at its maximum and minimum lengths. As can be seen in the figure, when kinematic redundancy is added to one of the legs, any prismatic length between L_{min} and L_{max} can be used for a specified pose of the end-effector, providing an infinite number of possible solutions to the inverse kinematics problem. This allows the orientation of the distal link A_1B_1 to be changed. Link A_1B_1 can thus have any orientation between the extreme positions shown. The orientation of A_1B_1 affects the orientation and the magnitude of the force applied at B_1 and therefore changes the force polygon. For a specified length O_1A_1, the vertices of the new polygon are still obtained when two actuator torques are at their maximum values.

3. Manipulator Kinematics

3.1. Inverse displacement solution

From Fig. 5, the vector loop produces

$$\mathbf{p} = \mathbf{OO}_i + \mathbf{O}_i\mathbf{A}_i + \mathbf{A}_i\mathbf{B}_i - \mathbf{PB}_i \tag{1}$$

where $\mathbf{p}$ is the vector expressing point P, the other vectors are from the point indicated by the first letter to the point indicated by the second letter and $i = 1, 2, 3$. It should be noted that $\mathbf{PB}_i = \mathbf{RPB}_i'$ and $\mathbf{R}$ is the rotation matrix $\begin{bmatrix} \cos\phi & -\sin\phi \\ \sin\phi & \cos\phi \end{bmatrix}$, specifying the orientation of the moving frame and $\mathbf{PB_i'}$ is the vector from P to B_i expressed in the moving frame xy. The vector $\mathbf{O}_i\mathbf{A}_i$ can be expressed as:

$$\mathbf{O}_i\mathbf{A}_i = \begin{bmatrix} L_i\cos\theta_i \\ L_i\sin\theta_i \end{bmatrix} \tag{2}$$

To eliminate $\mathbf{A}_i\mathbf{B}_i$, Eq. (1) can be rearranged as:

$$\mathbf{A}_i\mathbf{B}_i = \mathbf{p} - \mathbf{OO}_i - \mathbf{O}_i\mathbf{A}_i + \mathbf{PB}_i \tag{3}$$

Squaring both sides yields

$$\mathbf{A}_i\mathbf{B}_i^T\mathbf{A}_i\mathbf{B}_i = l^2 = (\mathbf{p} - \mathbf{OO}_i - \mathbf{O}_i\mathbf{A}_i + \mathbf{PB}_i)^T(\mathbf{p} - \mathbf{OO}_i - \mathbf{O}_i\mathbf{A}_i + \mathbf{PB}_i) \tag{4}$$

Eq. (4) can be written as:

$$l^2 = (\mathbf{w}_i - \mathbf{O}_i\mathbf{A}_i)^T(\mathbf{w}_i - \mathbf{O}_i\mathbf{A}_i) \tag{5}$$

where:

$$\mathbf{w}_i = \mathbf{p} - \mathbf{OO}_i + \mathbf{PB}_i \tag{6}$$

https://doi.org/10.1017/S0263574720001381 Published online by Cambridge University Press

Setting $\mathbf{O}_i\mathbf{A}_i^T\mathbf{O}_i\mathbf{A}_i = L_i^2$ and rearranging Eq. (5) yields

$$2\mathbf{w}_i^T\mathbf{O}_i\mathbf{A}_i = \mathbf{w}_i^T\mathbf{w}_i + L_i^2 - l^2 \tag{7}$$

Note that the right-hand side of Eq. (7) is completely known. Eq. (7) can be rewritten as:

$$A\cos\theta_i + B\sin\theta_i + C = 0 \tag{8}$$

where

$$\begin{aligned} A &= 2\mathbf{w}_i^T\mathbf{e}_1 L_i \\ B &= 2\mathbf{w}_i^T\mathbf{e}_2 L_i \\ C &= l^2 - L_i^2 - \mathbf{w}_i^T\mathbf{w}_i \end{aligned} \tag{9}$$

and

$$\begin{aligned} \mathbf{e}_1 &= \begin{bmatrix} 1 \\ 0 \end{bmatrix} \\ \mathbf{e}_2 &= \begin{bmatrix} 0 \\ 1 \end{bmatrix} \end{aligned} \tag{10}$$

Using the tangent half-angle substitution $T_i = \tan\frac{\theta_i}{2}$ allows Eq. (8) to be rewritten as:

$$(C - A)T_i^2 + 2BT_i + (C + A) = 0 \tag{11}$$

which has two roots for each θ_i.

With the angles θ_i determined, the unit vector $\mathbf{n}_{i1}$ along the proximal link O_iA_i is obtained as:

$$\mathbf{n}_{i1} = \begin{bmatrix} \cos\theta_i \\ \sin\theta_i \end{bmatrix} \tag{12}$$

The unit vector $\mathbf{n}_{i2}$ along link A_iB_i can also be determined as:

$$\mathbf{n}_{i2} = \frac{\mathbf{OB}_i - \mathbf{OA}_i}{l} = \frac{(\mathbf{p} + \mathbf{PB}_i) - \mathbf{OA}_i}{l} \tag{13}$$

3.2. Force analysis

The required forces can be determined from the equilibrium equations. Let $\mathbf{f}_i$ designate the force directed along the distal link of leg i on the end-effector, that is, the force along link A_iB_i of magnitude $\mathbf{f}_i$. The forces acting on the end-effector are shown in Fig. 7. The equilibrium equations on the end-effector lead to:

$$\begin{bmatrix} \mathbf{n}_{12} & \mathbf{n}_{22} & \mathbf{n}_{32} \\ \mathbf{z}^T(\mathbf{PB}_1 \times \mathbf{n}_{12}) & \mathbf{z}^T(\mathbf{PB}_2 \times \mathbf{n}_{22}) & \mathbf{z}^T(\mathbf{PB}_3 \times \mathbf{n}_{32}) \end{bmatrix} \begin{bmatrix} f_1 \\ f_2 \\ f_3 \end{bmatrix} = \begin{bmatrix} \mathbf{f}_e \\ m_{ez} \end{bmatrix} \tag{14}$$

where $\mathbf{f}_e$ represents the force applied by the end-effector and m_{ez} represents the moment about point P applied by the end-effector.

Eq. (14) can be rewritten as:

$$\mathbf{J}_2^T\boldsymbol{\tau}_2 = \mathbf{F} \tag{15}$$

where $\boldsymbol{\tau}_2$ is the vector of forces in the distal links, $\mathbf{F}$ represents the end-effector output force and moment, or wrench, and $\mathbf{J}_2^T$ is the transpose of the manipulator Jacobian matrix that relates these two quantities. If the output wrench is specified, the axial forces in the distal links can be determined with:

$$\boldsymbol{\tau}_2 = \mathbf{J}_2^{-T}\mathbf{F} \tag{16}$$

https://doi.org/10.1017/S0263574720001381 Published online by Cambridge University Press

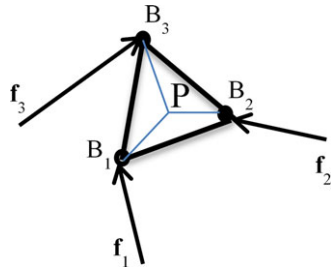

Fig. 7. Forces acting on the end-effector

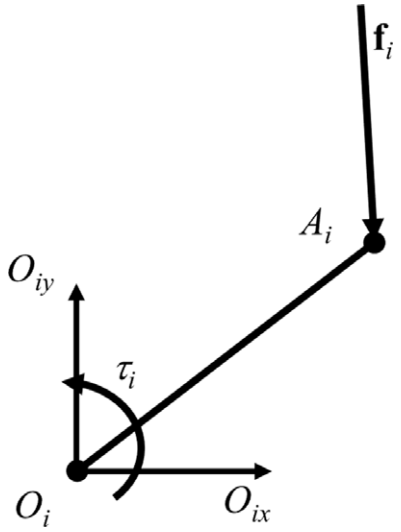

Fig. 8. Forces acting on proximal link $O_i A_i$.

The actuator torques required at the base can be obtained using the equilibrium conditions of the base proximal links $O_i A_i$. Figure 8 shows the forces acting on link $O_i A_i$ where $\mathbf{f}_i$ is the reaction force at A_i on link $O_i A_i$.

If $\mathbf{n}_{i1}$ designates a unit vector from O_i to A_i, the torque required can be found from the magnitude of the moment $\boldsymbol{\tau}_i$, that is, τ_i, computed by summing the moments about O_i:

$$\tau_i = -L_i \mathbf{z}^T (\mathbf{n}_{i1} \times \mathbf{f}_i) = -L_i \mathbf{z}^T (\mathbf{n}_{i1} \times f_i(-\mathbf{n}_{i2})) = L_i f_i \mathbf{z}^T (\mathbf{n}_{i1} \times \mathbf{n}_{i2}) \tag{17}$$

where L_i is the distance between O_i and A_i, and $\mathbf{f}_i$ is in the opposite direction of $\mathbf{n}_{i2}$.

Since both vectors in Eq. (17) are about the z-axis, the force f_i in the distal link corresponding to a specified torque can be obtained with:

$$f_i = \frac{\tau_i}{L_i \mathbf{z}^T (\mathbf{n}_{i1} \times \mathbf{n}_{i2})} \tag{18}$$

The magnitude of the force in the proximal link, designated as f_{act_i}, can be obtained by the projection of $\mathbf{f}_i$ in the direction of $O_i A_i$:

$$f_{act_i} = \mathbf{f_i}^T \mathbf{n}_{i1} \tag{19}$$

4. Procedure to Determine Wrench Performance

4.1. Methodology

The wrench capabilities of a non-redundant planar parallel manipulator depend on the different combinations of actuators at their maximum capacities.[18,20] Eq. (14) is in the form $\mathbf{Ax} = \mathbf{b}$. This equation

https://doi.org/10.1017/S0263574720001381 Published online by Cambridge University Press

can be solved when there are no more than three unknowns. Depending on the combination of actuators at their maximum capabilities, Eq. (14) can be rearranged such that matrix **A** and vector **b** contain only known quantities and **x** can be solved for. To illustrate this, let us consider the case to determine the force polygon when a prescribed moment is applied to the end-effector.

It was shown in Firmani et al.[18] that the coordinates of the points of the force polytope could be obtained without computing them at discretized angles that varied from 0 to 2π. As stated previously, for a given combination of lengths, the vertices of the force polygon occur when two actuator torques are at their maximum values. The polytope can be obtained by checking the 12 possible combinations of maximum torques. There are three combinations of torques at their maximum values (two out of three branches are at their maximum torques) and for each of those combinations, there are four cases of torques at their positive and negative maximum values ($\pm\tau_{i_{max}}$, $\pm\tau_{j_{max}}$). For a specified applied moment m_{ez} at a given pose, and the case where two actuators are at their maximum values, there are three unknowns in Eq. (14): the values of the components f_x and f_y of the force applied at the end-effector and the force in the leg in which the actuator is not maximized, denoted as f_k. The latter will be henceforth designated as the force in transition.

Let i, j, and k denote the three legs of the manipulator and consider the case where the torques are maximum in legs i and j. Eq. (14) can be rewritten in the following form:

$$\begin{bmatrix} \mathbf{n}_{i2} & \mathbf{n}_{j2} & \mathbf{n}_{k2} \\ \mathbf{z}^T(\mathbf{PB}_i \times \mathbf{n}_{i2}) & \mathbf{z}^T(\mathbf{PB}_j \times \mathbf{n}_{j2}) & \mathbf{z}^T(\mathbf{PB}_k \times \mathbf{n}_{k2}) \end{bmatrix} \begin{bmatrix} f_{imax} \\ f_{jmax} \\ f_k \end{bmatrix} = \begin{bmatrix} \mathbf{f}_e \\ m_{ez} \end{bmatrix} \tag{20}$$

where f_{imax} and f_{jmax} correspond to the forces in the distal links produced by the maximum torques in legs i and j, respectively. This equation can be rearranged as:

$$\begin{bmatrix} -1 & 0 & n_{k2_x} \\ 0 & -1 & n_{k2_y} \\ 0 & 0 & \mathbf{z}^T(\mathbf{PB}_k \times \mathbf{n}_{k2}) \end{bmatrix} \begin{bmatrix} f_x \\ f_y \\ f_k \end{bmatrix} = \begin{bmatrix} -\mathbf{n}_{i2} f_{imax} - \mathbf{n}_{j2} f_{jmax} \\ -\mathbf{z}^T(\mathbf{PB}_i \times \mathbf{n}_{i2}) f_{imax} - \mathbf{z}^T(\mathbf{PB}_j \times \mathbf{n}_{j2}) f_{jmax} + m_{ez} \end{bmatrix} \tag{21}$$

Eq. (21) is of the form $\mathbf{Ax} = \mathbf{b}$ where **A** and **b** are known and **x** can be solved for. The values of f_x and f_y are the coordinates of a point of the polygon. Any combination of maximum torques that produces a force in leg k that exceeds the maximum force that can be exerted by the actuator of leg k, f_{kmax}, is not possible and is removed from the list of potential vertex points. It should be noted that the computation of a possible vertex point involves only the resolution of three equations, each with one unknown. The last row of Eq. (21) has only one unknown, f_k, and can be solved first, leaving only one unknown for each of the equations in the first two rows.

Other force capabilities analyses can be performed using a similar methodology.

4.2. Effect of redundancy in one of the branches on the vertex points

Prior to explaining the procedure to obtain the force polygon when all the proximal link lengths vary, let us examine what happens to the polygon when two lengths are kept fixed and the other is varied from its minimum to its maximum length. Figure 9 shows the case where four polygons are generated for the four combinations of proximal link lengths indicated. The case presented is for an applied moment $m_{ez} = 0$ and is therefore a pure force analysis. In all cases, the length of the proximal link in the first and third legs is kept constant at 0.15 m. The length of the proximal link of the second leg is varied using four lengths that are between 0.15 and 0.25 m. When all the lengths are equal, one can note that the polygon (in blue) shows elements of symmetry since the force applied by links $A_i B_i$, i = 1,2,3 are equal when the extreme values of the torques are equal. When the length of link 2 changes, the force applied on the end-effector by link $A_2 B_2$ changes and the polygons are no longer symmetric.

In the upper right (and lower left) of the figure, there are four points that were obtained for each polygon generated. A dotted line was added between the points obtained at the extreme positions of leg 2 (0.15 and 0.25 m). This line passes through all points generated for polygons with proximal link lengths for the second leg between 0.15 and 0.25 m. This important result allows one to conclude that

https://doi.org/10.1017/S0263574720001381 Published online by Cambridge University Press

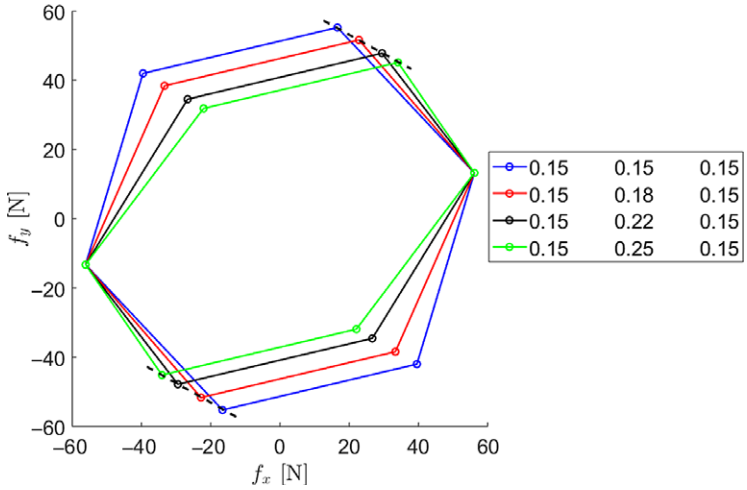

Fig. 9. Effect of redundancy on the force polygon.

a straight line can be drawn between the points obtained at the extreme positions and that that line will contain any points for an intermediate length. The force polygon is thus composed of the outermost lines in the figure and the dotted lines, since there is an intermediate length that corresponds to a point on the dotted line. It should be noted from Fig. 4 that each vertex corresponds to a case where two actuators are at their maximum capacity, and that the straight lines drawn between the points obtained at the extreme positions in Fig. 9 connect two points with the same actuators at their maximum capacity.

When redundancy is included in all legs, the force polygon can be obtained by computing the forces for all combinations that include only the extreme positions of the proximal link lengths. For three legs, there are, therefore, only eight possible combinations of proximal link lengths to verify. Once the forces for all combinations are computed, the force polygon can be produced. In the results that follow, the end-effector pose is $x = 0$, $y = 0$, and $\phi = 0$. Four different wrench capabilities are examined.

5. Wrench Capabilities of the 3-RPRR Manipulator

5.1. Pure force analysis

The first case studied is a pure force analysis ($m_{ez} = 0$). This is the case studied in Weihmann et al.[23] and allows a comparison with the only known published results to obtain the force polygon of a kinematically redundant parallel manipulator. As stated in the previous section, the force polygon corresponding to each of the eight combinations that correspond to the extreme positions can be found. The outermost points are joined by straight lines to produce the force polygon for the redundant manipulator. This can be done with a convex hull operation for a pure force analysis.

The procedure to obtain the force polygon is

1. Specify the pose $\mathbf{p}$ and compute the coordinates of point B using $\mathbf{p} + \mathbf{RPB}_i'$.
2. Compute vectors $\mathbf{OO}_i$.
3. Compute $\mathbf{w}_i$ using Eq. (6) (note that $\mathbf{p} + \mathbf{RPB}_i$ has been computed in Step 1).
4. Compute A, B, and C using Eq. (9) and solve Eq. (11) to determine the two solutions for θ_i. Choose the solution that corresponds to the selected leg layouts.
5. Compute unit vectors $\mathbf{n}_{i1}$ and $\mathbf{n}_{i2}$ using Eqs. (12) and (13). $\mathbf{O}_i\mathbf{A}_i$ is obtained from Eq. (2).
6. Compute the coordinates of the vertices of the polygon using the 12 possible combinations of 2 actuator torques that are maximized $\pm\tau_{i_{max}}$, $\pm\tau_{j_{max}}$ using Eq. (21). Note that f_{imax} and f_{jmax} are obtained from Eq. (18) using the maximum torque value.
7. Remove any combination that produces a force in transition larger than the maximum possible force produced by its actuator.
8. Perform a convex hull operation to obtain the points of the force polygon. The function `convhull` in MATLAB can be used to generate the convex hull of the points.

https://doi.org/10.1017/S0263574720001381 Published online by Cambridge University Press

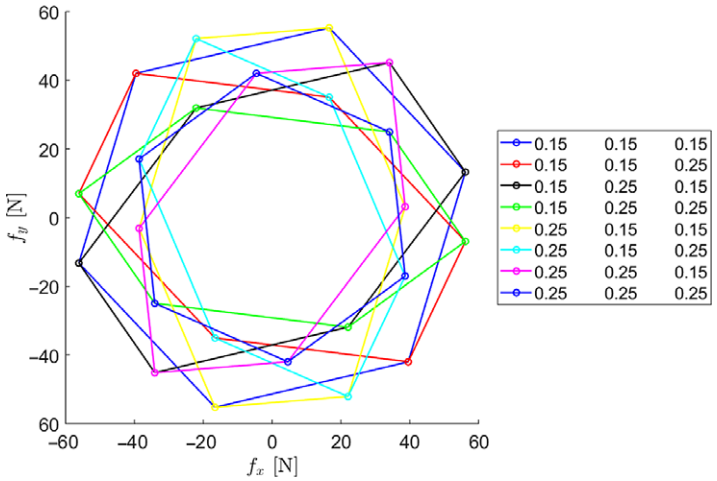

Fig. 10. Force polygons for eight possible proximal link length combinations.

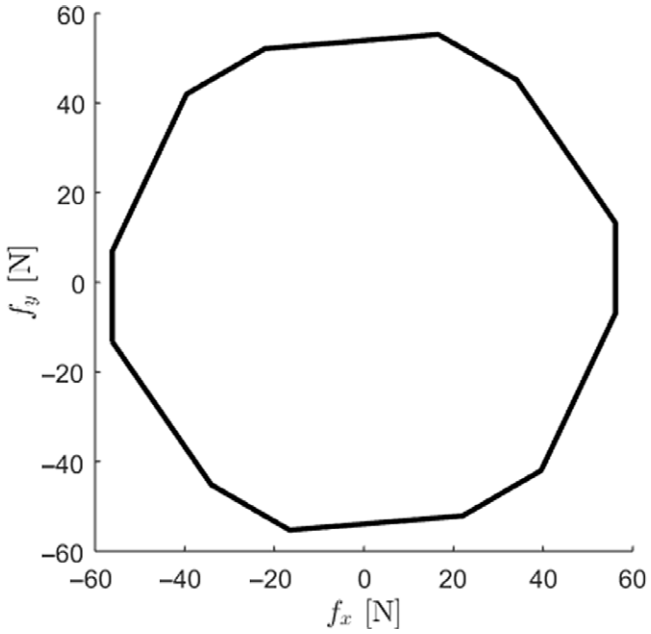

Fig. 11. Force polygon for the 3-RPRR.

Using this procedure, the complete force polygon for the 3-RPRR kinematically redundant planar parallel manipulator can be generated. Figure 10 shows the force polygons for the eight possible cases of extreme proximal link lengths and Fig. 11 shows the complete force polygon for the 3-RPRR. Comparing Fig. 11 to the results from Weihmann et al.[23] shows that the generated force polygon is the same. However, unlike the results from Weihmann et al.,[23] that are an approximation of the force polygon due to the use of optimization, the results shown in Fig. 11 are an exact solution. The solution presented here is very efficient compared to the method used by Weihmann et al..[23] In the latter, a polar discretization from 0° to 360° was used to produce the polygon. For each discretized direction, a coordinate for the force polygon is obtained using a Differential Evolution optimization, a procedure computationally expensive. Also, the resulting polygon does not consist of nice straight lines, since each point computed is an approximate solution. The procedure presented here requires only to solve Eq. (21) for the eight proximal link length combinations that correspond to the links' extreme positions while excluding any torque combinations that produce transition forces that exceed the maximum torque capacity of the torque in transition. The plot of the torques required to produce the force polygon is presented in Fig. 12 where angle α is the angle shown in Fig. 4. The plot is the same as that obtained by Weihmann et al..[23]

https://doi.org/10.1017/S0263574720001381 Published online by Cambridge University Press

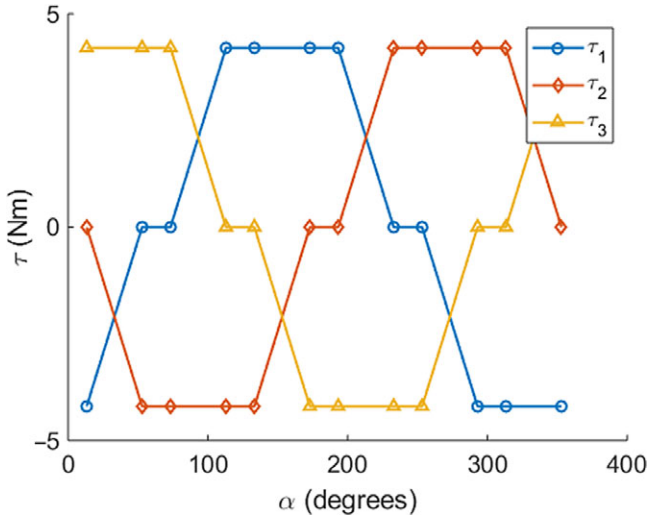

Fig. 12. Joint torques versus α for the 3-RPRR.

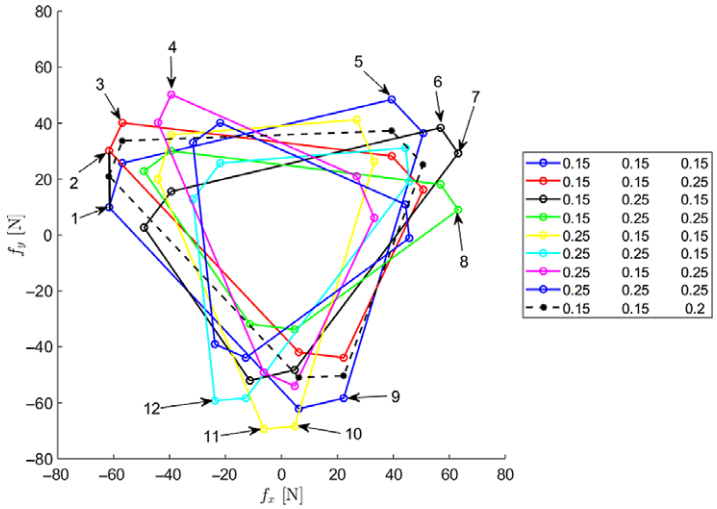

Fig. 13. Force polygons for eight possible proximal link length combinations with an applied moment of 2 Nm.

An important observation can be deduced about the force polygons for kinematically redundant planar parallel manipulators. For a non-redundant manipulator, a line on the force polygon indicates that one actuator is at its maximum capacity while two are at their maximum capacity at a vertex of the polygon.[29] For a kinematically redundant manipulator, this is not necessarily the case. Two actuators are at their maximum capacity on the lines that are generated when one of the proximal link lengths is transitioning between its two extreme positions and the other two proximal link lengths are at one of their extreme positions, as illustrated in Fig. 9. This is also illustrated in Fig. 12, where, for example, two torques are at their maximum values when α is between approximately 50° and 75°.

If one considers the area within the force polygon as an indicator of the performance of a manipulator, the area in the polygon shown in Fig. 11 has an area 11.6% larger than that of the polygon that corresponds to a non-redundant manipulator with all proximal legs equal to 0.15 m (one of the eight polygons shown in Fig. 10).

5.2. Maximum force with a prescribed moment

The second wrench performance studied allows the determination of the force polygon for a prescribed (specified) moment that is not null. In this case, the force polygon is no longer convex as was the case for a pure force analysis. Figure 13 shows the force polygons for the eight possible cases of extreme proximal link lengths when a moment of 2 Nm is prescribed. The polygon with the dashed

https://doi.org/10.1017/S0263574720001381 Published online by Cambridge University Press

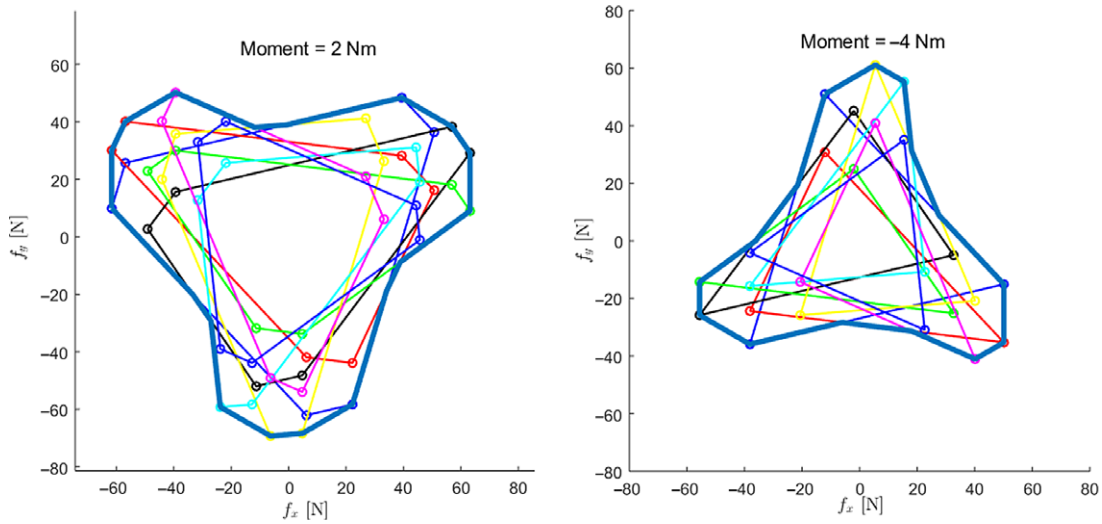

Fig. 14. Force polygons for applied moments of 2 and −4 Nm.

line represents the force polygon for an intermediate length. The outermost vertices that determine the convex shape of the eight polygons are numbered. Recall from the previous section that two actuators are at their maximum values at a vertex. At vertices 1 and 2, the same two actuators are at their maximum values. As was explained in the previous section, a straight line can be drawn between these points and a point on this line will correspond to an intermediate length of one of the proximal links. A straight line is added between points 1 and 2 and it is seen to pass through one of the vertex points of the polygon for an intermediate length. In the figure, the following group of vertices have the same actuators at their maximum capacity: (1, 2, 3, and 4), (5, 6, 7, and 8), and (9, 10, 11, and 12). It should be noted that these 12 vertices are found using the same method as when no moment is applied. However, a straight line cannot be drawn between vertices 4 and 5, for example, to produce the correct force polygon.

The procedure to obtain the force polygon when a moment is prescribed is:

1. Repeat steps 1–7 in subsection 5.1.
2. Determine the vertices that compose the convex shape of the combination of the eight force polygons.
3. For $i = 1$ to n, where n corresponds to the last vertex, identify the two torques that are at their maximum values for each vertex i, that is, $(\tau_{i_{max1}}, \tau_{i_{max2}})$.
4. For $i = 1$ to n and for vertex n and vertex 1, if $(\tau_{i_{max1}}, \tau_{i_{max2}}) = (\tau_{i+1_{max1}}, \tau_{i+1_{max2}})$.
   a. join them by a straight line;
   b. else determine the intersection points of the outermost lines and keep the portions of these lines between the vertex points i and $i + 1$.
5. Join all lines to obtain the force polygon.

When the above procedure is applied to Fig. 13, consecutively numbered vertices from 1–4 are joined by straight lines since they have the same combination of actuator torques at their maximum capacity. The latter is not the case between vertices 4 and 5, so the intersections of the outermost lines are determined and the outermost portions of the lines between vertices 4 and 5 constitute the boundary of the force polygon between these two vertices. Consecutively numbered vertices from 5 to 8 are then also joined by straight lines since they have the same combination of actuator torques at their maximum capacity. The procedure is repeated until vertex 1 is reached. Figure 14 shows the resulting force polygons when this procedure is applied with moments of 2 and −4 Nm. The thick outer lines represent the maximum force corresponding to the applied moment. The legend is not shown due to space limitations, but it is the same as in the previous figures. The areas enclosed within the outside polygons in Fig. 14 are 29.3% (m = 2 Nm) and 57.3% (m = −4 Nm) larger than that of the polygons obtained with a non-redundant manipulator with all proximal legs equal to 0.15 m.

https://doi.org/10.1017/S0263574720001381 Published online by Cambridge University Press

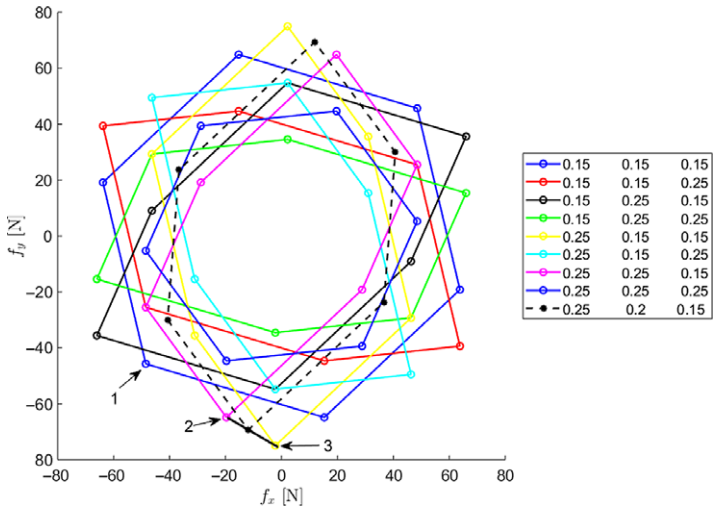

Fig. 15. Force polygons maximum reachable force.

5.3. Maximum reachable force

This case provides information on the maximum forces that the manipulator can apply or sustain. There is a moment associated with the maximum reachable force. As shown by Firmani et al.,[18] for a non-redundant manipulator, the maximum reachable force occurs when all three actuators are at their maximum values. There are eight combinations of maximum torques ($\pm$) for a given set of extreme lengths. When three actuators are at their maximum capacity, the force f_k becomes f_{kmax} in Eq. (20). The maximum force and associated moment are therefore obtained directly. Of the eight combinations, six will provide the vertices of the polygon providing the maximum reachable force. The other two combinations produce a point that is inside the polygon.

Figure 15 shows the eight polygons produced by the extreme length combinations. Also shown is a polygon corresponding to an intermediate length. In this figure, the vertices 1 and 2 do not have the same actuators at their maximum capacity, but vertices 2 and 3 do. When two consecutive vertices correspond to the same combination of torques being at their maximum capacities, a line can be drawn between them. There exists an intermediate length that corresponds to a point along this line. The figure shows a line drawn between vertices 2 and 3 and one of the vertices of the intermediate length for the second leg is on this line. The second leg is transitioning from a length of 0.15 to 0.25 m along this line. The procedure to obtain the complete maximum reachable force polygon is very similar to the procedure to obtain the polygon for a prescribed moment shown in Subsection 5.2. The only difference is in steps 4 and 5, where each vertex corresponds to a combination of three torques at their maximum capabilities instead of two. When this procedure is applied and lines are added when two vertices correspond to the same combination of actuators at their maximum capacity, the maximum reachable force polygon can be found as shown in Fig. 16. The distance between the center of the polygon ($f_x = 0$ and $f_y = 0$) and any point on the boundary of the polygon represents the largest force that can be applied in the direction of that point. A moment needed to satisfy equilibrium will be associated with this force. The increase in area of this polygon compared to the area of the polygon obtained for a non-redundant manipulator with proximal legs of 0.15 m is 21.4%.

5.4. Maximum moment with a prescribed force

For a prescribed force, there exists a range of moments that can be applied. It was shown by Firmani et al.[18] that for a non-redundant manipulator, this condition corresponds to one actuator being at its maximum capacity. When f_x and f_y are specified, and knowing that one actuator is at its maximum capacity, Eq. (14) can be rearranged in the form $\mathbf{Ax} = \mathbf{b}$. The unknown vector is $\mathbf{x} = [m_{ez}\ f_j\ f_k]^T$ where m_{ez} is the unknown moment and f_j and f_k are the forces in the legs that do not have an actuator at its maximum capacity, that is, forces in transition. There are six conditions of maximum torques to be verified when only one actuator is at its maximum capacity, each actuator evaluated at positive and negative values. Only two torques will keep the other forces in transition within the maximum allowable actuator forces. Therefore, for a specified value of f_x and f_y, there will be a

https://doi.org/10.1017/S0263574720001381 Published online by Cambridge University Press

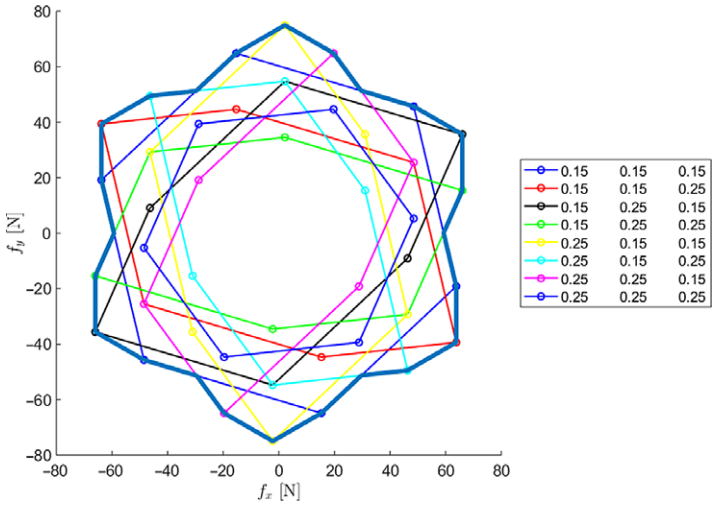

Fig. 16. Maximum reachable force polygon.

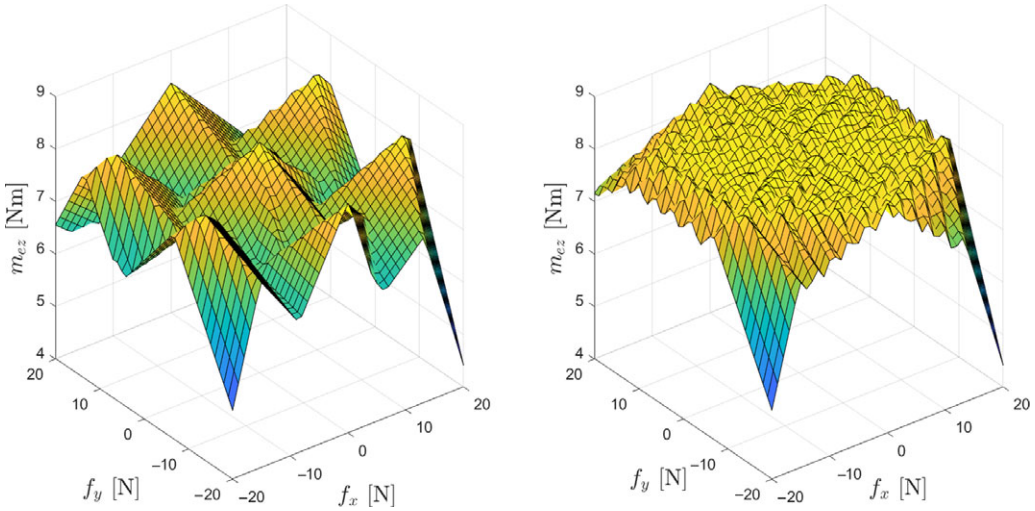

Fig. 17. Effect of intermediate lengths on maximum moment for a prescribed force.

minimum and a maximum value of the moment that can be applied, and the manipulator can apply (or sustain) any moment within this range. It should be noted that for any value of (f_x, f_y) located on the polygon indicated in Fig. 16, there is only one value for the moment.

This problem is more difficult to apply to the kinematically redundant manipulator. For a specified force, there is an intermediate length that may provide a range of moments that is larger than that obtained with the extreme lengths. This can be observed in Fig. 15. On the line between vertices 2 and 3, no moment is found to be possible when only the extreme lengths are used, but there is an intermediate length that produces this moment.The same situation occurs when we consider the entire region in which a specified force has an associated range of moments. It is therefore not possible to obtain the exact solution based only on the extreme length combinations. This can be seen in Fig. 17. The prescribed force was discretized from −20 to 20 N for both f_x and f_y in increments of 1 N and the maximum value of the moment was computed at each point. For clarity, the minimum value of the moment is not shown. The figure on the left used only the eight extreme lengths, while the one on the right used the 216 combinations in which the lengths range from 0.15 to 0.25 m in increments of 0.2 m. One can clearly see that some intermediate lengths produce moments that are larger than those found using only the extreme lengths.

The plane of f_x and f_y was discretized between −75 and +75 N in both directions in increments of 1 N. At each location, the minimum and maximum moments were computed. Figure 18 shows a

https://doi.org/10.1017/S0263574720001381 Published online by Cambridge University Press

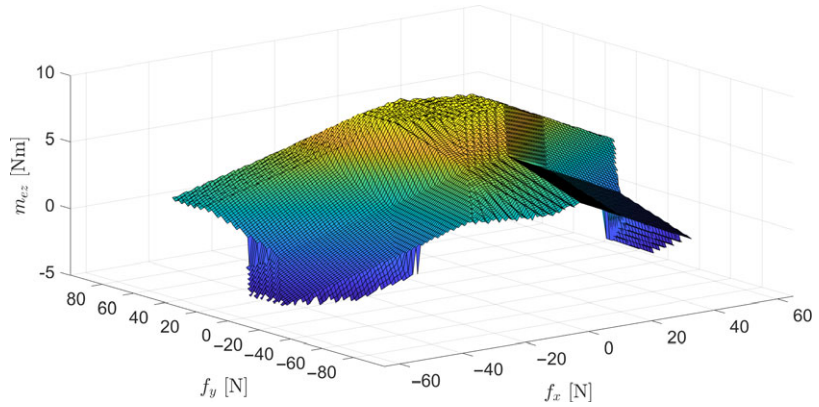

Fig. 18. Maximum moment for a prescribed force throughout the workspace.

surface of the maximum values when the intermediate lengths designated in the previous paragraph are used. This provides an approximate solution of the maximum moment throughout the workspace.

6. Conclusions

This paper presented a methodology to obtain several wrench performances of a kinematically redundant planar parallel manipulator using a wrench polytope approach. The latter had been previously used to determine the explicit solution of the force capabilities for non-redundant planar parallel manipulators[18] and for planar parallel manipulators with actuation redundancy.[22]

As mentioned previously, only one other work found in the literature[23] had proposed a solution for a pure force analysis of a kinematically redundant planar parallel manipulator, but that work used optimization. This paper presented a methodology that produces an explicit solution for the same pure force analysis. The methodology was tested on the same problem to verify that the results matched those of Weihmann et al..[23] The procedure presented here is exact and, being explicit, very efficient.

Contrary to the force polygons of non-redundant manipulators in which a line on the polygon corresponds to one actuator being at its maximum capacity, some lines on the force polygon of kinematically redundant manipulators correspond to the case where two actuators are at their maximum capacity.

Three other cases of wrench performance for a kinematically redundant manipulator were studied. The proposed methodology also produces the exact solution for the maximum force with a prescribed moment, and for the maximum reachable force. The solution for the maximum moment for a prescribed force is approximate. The precision of this solution can be increased by including more intermediate lengths. The method presented is very efficient compared to an optimization approach. The latter three cases were analysed for the first time for a manipulator with kinematic redundancy.

An efficient method to obtain the force capabilities is very useful in a design context. The effect of modifying design parameters such as the proximal link lengths, the range of the prismatic joints, or the maximum torque capacities can be rapidly observed and the performance of the manipulator can be improved to obtain desired results.

References

1. S. Nokleby, R. Fisher, R. Podhorodeski and F. Firmani, "Force capabilities of redundantly-actuated parallel manipulators," *Mech. Mach. Theory* **40**(5), 578–599 (2005).
2. C. Gosselin and J. Angeles, "Singularity analysis of closed-loop kinematic chains," *IEEE Trans. Robot. Automat.* **6**(3), 281–290 (1990).
3. K. Zanganeh and J. Angeles, "Instantaneous Kinematics and Design of a Novel Redundant Parallel Manipulator," **In**: *Proceedings of IEEE Conference on Robotics and Automation* (1994) pp. 3043–3048.
4. J. Wang and C. Gosselin, "Kinematic analysis and design of kinematically redundant parallel mechanisms," *ASME J. Mech. Des.* **126**(1), 109–118 (2004).
5. M. G. Mohamed and C. M. Gosselin, "Design and analysis of kinematically redundant parallel manipulators with configurable platforms," *IEEE Trans. Robot.* **21**(3), 277–287 (2005).
6. I. Ebrahimi, J. A. Carretero and R. Boudreau, "3-PRRR redundant planar parallel manipulator: Inverse displacement, workspace and singularity analyses," *Mech. Mach. Theory* **42**(8), 1007–1016 (2009).

https://doi.org/10.1017/S0263574720001381 Published online by Cambridge University Press

7. S.-H. Cha, T. A. Lasky and S. A. Velinsky, " Determination of the kinematically redundant active prismatic joint variable ranges of a planar parallel mechanism for singularity-free trajectories," *Mech. Mach. Theory* **44**(5), 1032–1044 (2009).
8. R. Boudreau and S. Nokleby, "Force optimization of kinematically-redundant planar parallel manipulators following a desired trajectory," *Mech. Mach. Theory* **56**(10), 138–155 (2012).
9. A. G. Ruiz, J. C. Santos, J. Croes, W. Desmet and M. M. da Silva, "On redundancy resolution and energy consumption of kinematically redundant planar parallel manipulators," *Robotica* **36**(6), 809–821 (2018).
10. C. Gosselin, T. Laliberté and A. Veillette, "Singularity-free kinematically redundant planar parallel mechanisms with unlimited rotational capability," *IEEE Trans. Robot.* **31**(2), 457–467 (2016).
11. L.-T. Schreiber and C. Gosselin, "Kinematically redundant planar parallel mechanisms: Kinematics, workspace and trajectory planning," *Mech. Mach. Theory* **119**, 91–105 (2018).
12. J.-P. Merlet, "Redundant parallel manipulators," *J. Lab. Robot. Automat.* **8**(1), 17–24 (1996).
13. S. Kock and W. Schumacher, "Parallel x-y Manipulator with Actuation Redundancy for High-Speed and Active-Stiffness Applications," **In**: *Proceedings of IEEE Conference on Robotics and Automation* (1998) pp. 2295–2300.
14. F. Firmani and R. Podhorodeski, "Force-unconstrained poses for a redundantly actuated planar parallel manipulator," *Mech. Mach. Theory* **39**(5), 459–476 (2004).
15. C. Gosselin and L.-T. Schreiber, "Redundancy in parallel mechanisms: A review," *ASME Appl. Mech. Rev.* **70**(1), 15 pages (2018).
16. T. Yoshikawa, "Manipulability of robotic mechanisms," *Int. J. Robot. Res.* **42**(2), 3–9 (1985).
17. T. Kokkinis and B. Paden, "Kinetostatic Performance Limits of Cooperating Robot Manipulators," **In**: *Proceedings of the ASME Winter Annual Meeting* (1989) pp. 151–155.
18. F. Firmani, A. Zibil, S. Nokleby and R. Podhorodeski, "Wrench capabilities of planar parallel manipulators - Part I: Wrench polytopes and performance indices," *Robotica* **26**(6), 791–802 (2008).
19. L. Mejia, H. Simas and D. Martins, "Force capability in general 3 DoF planar mechanisms," *Mech. Mach. Theory* **26**, 120–134 (2015).
20. A. Zibil, F. Firmani, S. Nokleby and R. Podhorodeski, "An explicit method for determining the force moment capabilities of redundantly actuated planar parallel manipulators," *ASME J. Mech. Des.* **129**(10), 1046–1055 (2007).
21. L. Mejia, H. Simas and D. Martins, "Wrench capability in redundant planar parallel manipulators with net degree of constraint equal to four, five or six," *Mech. Mach. Theory* **105**, 58–79 (2016).
22. F. Firmani, A. Zibil, S. Nokleby and R. Podhorodeski, "Wrench capabilities of planar parallel manipulators - Part II: Redundancy and wrench workspace analysis," *Robotica* **26**(6), 803–815 (2008).
23. L. Weihmann, D. Martins and L. Coelho, "Force capabilities of kinematically redundant planar parallel manipulators," **In**: *Proceedings of 13th World Congress in Mechanism and Machine Science* (2011) 8 pages.
24. R. Boudreau, S. Nokleby and M. Gallant, "Investigating the Wrench Capabilities of a Kinematically-Redundant Planar Parallel Manipulator," **In**: *Proceedings of the 2019 CCToMM Symposium on Mechanisms, Machines and Mechatronics* (2019) 12 pages.
25. C. Gosselin and J. Angeles, "The optimum kinematic design of a planar three-degree-of-freedom parallel manipulator," *J. Mech. Trans. Automat. Des*. **110**(1), 35–41 (1988).
26. I. A. Bonev, D. Zlatanov and C. Gosselin, "Singularity analysis of 3-DOF planar parallel mechanisms via screw theory," *J. Mech. Des.* **125**(3), 573–581 (2003).
27. M. Arsenault and R. Boudreau, "The synthesis of three-degree-of-freedom planar parallel mechanisms with revolute joints (3-RRR) for an optimal singularity-free workspace," *J. Robot. Syst.* **21**(5), 259–274 (2004).
28. S. Kucuk, "Simulation and design tool for performance analysis of planar parallel manipulators," *Simulation*. **88**(5), 542–556 (2012).
29. F. Firmani, A. Zibil, S. Nokleby and R. Podhorodeski, "Force-moment capabilities of revolute-jointed planar parallel manipulators with additional actuated branches," *Trans. CSME* **31**(4), 469–482 (2007).

https://doi.org/10.1017/S0263574720001381 Published online by Cambridge University Press